Preparation of thermally recyclable γ-alumina nanoparticles from boehmite for adsorption of anionic dyes: Spectrophotometric study, structural characterization and industrial experience

Amir Hossein Razm*, Amin Salem*,**,†, and Shiva Salem***

*Faculty of Chemical Engineering, Sahand University of Technology, Tabriz, Iran
**Center of Excellence for Color Science and Technology, Tehran, Iran
***Faculty of Chemical Engineering, Urmia University of Technology, Urmia, Iran

Abstract−γ-Alumina powders were produced from the calcination of pseudo-boehmite for scavenging anionic blue (RS 150), and red (RB 133) dyes. The effects of calcination temperature, soaking time, pH, and nanoparticle dosage on dye adsorption were investigated to fabricate a reusable adsorbent. The mentioned dyes can be efficiently adsorbed over the γ-alumina nanoparticles if the calcination conditions, and pH are identified correctly. The powder calcined at 700 °C within 30 min inherently exhibited a high affinity towards blue dye at pH 5.0, while the proper adsorption towards red dye was achieved at pH 2.0. The maximal blue, and red dye adsorption capacities were determined to be 303, and 417 mg L^{-1}, respectively. Although the calcination of boehmite at 1,000 °C led to the higher chemical resistance, the specific surface area significantly decreased from 202 to 126 m^2 g^{-1}, causing a significant drop in the adsorption of blue dye due to an increase in pore diameter, 6 nm. Importantly, the adsorptive performance of produced powder was stable with ten times thermal regeneration. Based on results obtained for the treatment of industrial textile wastewater, the fabricated γ-alumina powder is promising material to adsorb the anionic dyes.

Keywords: γ-Alumina Nanoparticles, Anionic Dyes, Adsorption, Thermal Stability, Reusability

INTRODUCTION

Water resource contamination by toxic streams discharged from textile industries is a serious environmental problem. The detrimental impacts of wastewater contaminated by anionic dyes are the main challenge from the environmental engineering viewpoint requiring eco-friendly innovation for the removal of these hazardous materials. On the other hand, the extended demand for clean water has led to governmental compulsion to recycle the treated wastewater. Moreover, the treatment of wastewater prevents jeopardizing human health, and ecological disturbances.

Anionic dyes are organic components which are dissociated into anions in water. These types of dyes, which are used to color wool, silk, and nylon, contain acidic groups like sulfate and carboxyl, providing the ionic bonds through the acid groups of dyes and the amine groups in the material. A variety of treatment methods have been innovated to remove the dyes from wastewater, including membrane separation [1], emulsion liquid membrane [2], chromatographic separation [3], coagulation [4], flocculation [5], and photocatalytic degradation [6]. The mentioned techniques are not attractive to remove anionic dyes from the wastewater in comparison to adsorption [7]. Low cost adsorbents like straw [8], fly ash [9], boron industry waste [10], wastes of soda ash plant [11], natural clay [12], and modified zeolite [13] have been used for the treatment of waste-

water contaminated with the anionic dyes. Notably, advanced materials, including functioned hollow glass microsphere [14], salicyl active esters [15], Cu$_3$SnS$_4$@C nanocomposite [16], amino-functionalized titanate nanotube [17], multifunctional carbon nanotube supported metal doped MnO$_2$ composite [18], organovermiculite-based adsorbent [19], chitosan [20], and magnetic multi-walled carbon nanotubes-Fe$_3$C nanocomposite [21] have been applied in the removal of anionic dyes due to the encouraging performance in the decontamination of pollutants. However, these materials have some limitations in terms of chemical resistance, regeneration, and reusability. Therefore, it is of great importance to undertake materials which could be regenerated after dye adsorption. Since dye removal is a solid-liquid interface phenomenon, as a result anion adsorption is largely influenced by textural features such as surface area, pore size, functional groups, and electrostatic forces.

Alumina is preferred to apply in aggressive environments due to excellent strength, hardness, and chemical resistance. This material commonly is formed in several crystalline structures as χ, κ, γ, δ, θ, η, and α forms. Alumina can be fabricated from gibbsite, Al(OH)$_3$, and or boehmite, AlOOH, by heat treatment [22,23]. Regardless, α-Al$_2$O$_3$, which is stable form, the other structures are metastable; therefore, the calcination process should be controlled to achieve a proper structure. During heat treatment, aluminum hydroxide is transformed into the metastable phase before converting into stable α-Al$_2$O$_3$. Due to existence of acidic sites in γ-Al$_2$O$_3$, this form of alumina is preferred for catalytic and adsorption purposes. The transformation from γ to α-Al$_2$O$_3$ leads to a decline in the number of active sites, which occurs in temperature above

1,000 °C [24]. The mesoporous γ-alumina fabricated by the template method has been used for the Congo Red removal from wastewater [25]. Reactive Red 120, and orange G were efficiently removed from solution by nano-sized alumina [26,27]. Alumina packed bed was used in the dynamic treatment of wastewater contaminated by reactive dyes [28]. Red 198, and Blue19 dyes were perfectly adsorbed onto alumina coated on multiwall carbon nanotubes [29].

Based on previous investigation, the γ-Al$_2$O$_3$ powder possessing large surface area, promises extended active sites for the adsorption. On the other hand, the chemical and thermal resistance of alumina provide a potential for application in the acidic environment, and thermal regeneration after treatment process. The identification operational constraints for the production and regeneration of γ-Al$_2$O$_3$ are of great importance from the industrial viewpoint to reuse without losing capacity in the deletion of anionic dyes from textile wastewaters. In the current work, a pseudo-boehmite powder, which is produced commercially, was chosen as a precursor to fabricate γ-Al$_2$O$_3$ powders. The obtained materials were first applied to treat the wastewater contaminated with the industrial anionic dyes, blue (RS 150), and red (RB 133), in the acidic environment. The proper conditions, including calcination temperature, soaking time, and pH, were determined to maximize the adsorption capacity. Finally, the spent adsorbent was thermally regenerated several times to evaluate the reusability of fabricated material in wastewater treatment. The integration of fabrication and regeneration constraints synergistically led to achieving an excellent scavenging capacity and easy thermal recovery.

MATERIALS AND METHODS

1. Materials

The commercial pseudo-boehmite powder, AlOOH, produced by Mineral Research Center of West Country in Iran, was purchased and utilized to prepare the adsorbents without further purification. Blue (RS 150) and red (RB 133) dyes were received from Khoy Textile Company Freudenberg, West Azerbaijan in Iran. Distilled water was employed for the preparation of dye stocks in which hydrochloric acid, 37%, was used to adjust the solution pH. The industrial wastewater contaminated by blue and red anionic dyes was collected from the discharged effluents of two textile factories which use from the selected dyes for fabric dyeing.

2. Fabrication of Adsorbents

Boehmite powder was first well dried within an electrical oven at 110 °C in air atmosphere for a day. The oven-dried powder was heated in an electrical furnace up to maximal temperatures, 500-1,000 °C, with a rate of 10 °C min^{-1}, and maintained at the mentioned temperatures for 15-120 min to obtain alumina powders. The thermally treated materials were allowed to cool naturally, ~50 °C, and then were placed in a desiccator until reaching room temperature.

3. Dye Removal Experiments

The concentrated stock solutions, 100 mg L^{-1}, were prepared by stirring dyes in the distilled water till dissolving completely. The stock solutions were further used to prepare solutions with different concentrations, 30-70 mg L^{-1}, by diluting to the required level. Hydrochloric acid solution, 0.5 mol L^{-1}, was used to adjust the pH

of solutions, and industrial wastewaters in the range of 2-6. Batch adsorption experiments of dyes onto alumina were conducted via magnetic agitating, 100 rpm, at 25 °C. Different content of adsorbents, 1.5-10.0 g L^{-1}, was immersed in the industrial wastewater to determine the proper dosage for recovery. The adsorbents were separated by centrifuge, 3,000 rpm, after 4 h, which is sufficient to achieve equilibrium. The removal process was evaluated by measuring the dye concentration using a Jenway UV-vis spectrophotometer (Model 6705, UK). A common route was applied to evaluate the adsorption of dye species. For the determination of dye concentration, six diluted solutions, 1 : 10, whose concentrations were known exactly, were used to identify a calibration plot. The absorbance spectra of standard solutions were then obtained by spectrophotometry. The blue and red dye solutions showed the maximal absorbance at wavelengths of 596, and 523 nm, respectively. The maximal absorbance of dye solutions was plotted versus concentration. The linearity of this plot arises from the Beer-Lambert law, which states that the absorption of light by dye is proportional to concentration in solution. The absorbance spectrum of each solution with unknown concentration was obtained to determine the dye content through the calibration plot. For the calculation of adsorption efficiency, R, and capacity, q$_e$, following equations were used:

$$R = \frac{(C_0 - C_e)}{C_0} \times 100 \tag{1}$$

$$q_e = \frac{(C_0 - C_e)V}{M} \tag{2}$$

where C$_0$, and C$_e$, mg L^{-1}, are the corresponding concentration of dye before and after adsorption, respectively, V is the solution or wastewater in milliliter, and M is the mass of adsorbent. The adsorption testes were repeated at least three times and the variance was calculated based on obtained data.

4. Thermal Regeneration of Adsorbents

By ten times repetition of the adsorption process, the sufficient content of spent adsorbent was collected to regenerate by thermal method. The collected wastes were transferred into the ceramic crucibles and heated at 500 °C in an electrical programmable kiln. The materials were heated with the rate of 10 °C min^{-1} up to 500 °C and kept at this temperature for 120 min. The regenerated adsorbents were cooled naturally to room temperature and placed in in a desiccator. The batch adsorption tests were carried out with regenerated adsorbent to examine the reusability of produced alumina.

5. Industrial Wastewater Properties

It is difficult to define a typical property for textile wastewater due to differences in the application techniques. Based on the data received from the textile industries, Table 1, the used wastewaters are a mix of dyes (Blue RS 150, or Red RB 133), and other pollutants, including solids, organics, and alkali metals. The concentration of dyes was determined by UV-vis spectrophotometry, using calibration plots. The pH, total suspended solids (TSS), chemical oxygen demand (COD), biochemical oxygen demand (BOD), and sodium concentration were monitored before discharging into environment. In the textile wastewater treatment, the dyes are first removed after solid separation. The biological, and chemical processes are carried out in another treatment plant to guarantee the

Table 1. Properties of industrial wastewater

Property	Blue wastewater	Red wastewater
pH	9.7	10.3
TSS (mg L^{-1})	370	440
COD (mg L^{-1})	1,100	1,030
BOD (mg L^{-1})	550	380
Na$^+$ (mg L^{-1})	6,800	7,500
Dye concentration (mg L^{-1})	70	82

safety of discharged water. In this study the solids were separated by centrifugation, and the dye adsorption was performed to evaluate the ability of adsorbents in treatment of wastewater.

6. Adsorbent Characterizations

Differential thermal analysis (DTA) and thermogravimetric (TG) study on boehmite powder were carried out in a ceramic crucible using a TA analyzer (DTA-TGA, Model Q600, USA) under air flow with a heating rate of 10 °C min^{-1}. The crystalline change occurring in the starting material with the calcination at different conditions were followed by Bruker D8-Advance (XRD, Karlsruhe, Germany) using Cu-Kα radiation in which the scanning rate was considered 0.02 $^\circ$s^{-1} in the 2θ range of 10-90°. Fourier transform infrared spectra analyses were performed on KBr discs in the range of 400-4,000 cm^{-1} using a Bruker FTIR spectrometer (Model Tensor 27, Germany). Scanning electron microscopy (SEM; Model 440I EOL, UK), and field emission scanning electron microscopy (FESEM; MIRA3, Tescan, Czech Republic) analyses were used for the morphological observations on gold coated surfaces. The nitrogen adsorption-desorption isotherms were collected at 77 K using a Quantachrome apparatus (Chem BET 3000, USA) to determine the textural properties and pore size distribution based on Brunauer-Emmett-Teller (BET), and Barrett-Joyner-Halenda (BJH) models, respectively. The zeta potential of adsorbents was measured by nanoPartica SZ-100V2 (Horiba, Ltd, Japan) instrument.

RESULTS AND DISCUSSION

1. Effect of Calcination Condition on Removal Efficiency

Fig. 1 shows the dye removal efficiency of thermally treated powders as a function of calcination temperature in which the pH of dye stocks was adjusted at 5.0. The yield of adsorption increased with the rise in calcination temperature, and remained at the constant level when the heat treatment was carried out in the range of 600-700 °C. Approximately 99 % of contaminants was removed by the powders calcined at 600-700 °C, which is necessary to satisfy the wastewater treatment. The removal efficiency plots show the same trend for the decontamination of dye solutions with a stable plateau in the range of 600-700 °C. However, a distinct decline in the yield appeared at temperatures above 700 °C. In comparison to blue dye adsorption efficiency, the excessive content of red dye could be adsorbed onto alumina powder heated at the temperatures higher than 700 °C, adversely affecting the decontamination performance.

To evaluate the effect of calcination time on dye removal efficiency, the boehmite powder was calcined at 700, and 1,000 °C in the soaking range of 15-120 min as displayed in Fig. 2. A unique
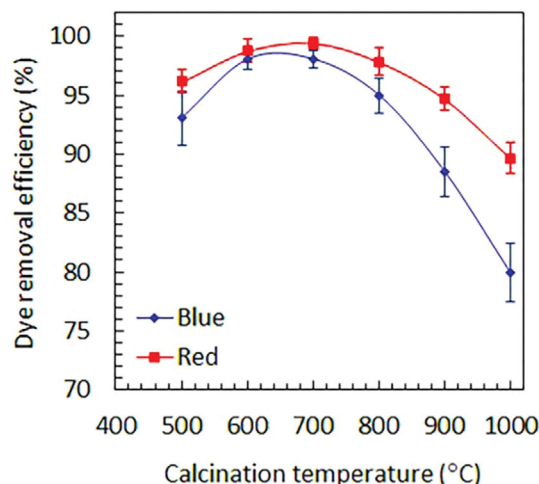

Fig. 1. Dye removal efficiency versus calcination temperature, soaking time: 120 min, dye concentration: 100 mg L^{-1}, pH: 5.0, and adsorbent dosage: 0.50 g L^{-1}.
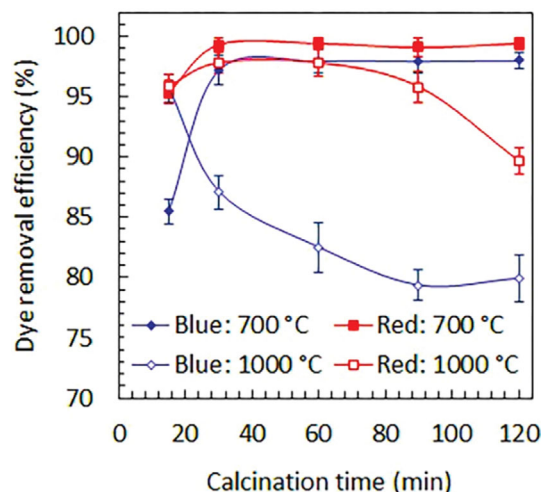

Fig. 2. Dye removal efficiency versus calcination time, soaking temperature: 700, and 1,000 °C, dye concentration: 100 mg L^{-1}, pH: 5.0, and adsorbent dosage: 0.50 g L^{-1}.

opportunity was provided to produce the adsorbent in the short time, which is beneficial from the economical point of view. The trend of efficiency is similar for two studied cases if the calcination temperature is adjusted at 700 °C, reaching to ~99% with soaking within 30 min remaining practically unchanged with treatment in the longer times. With adjustment of calcination temperature at 1,000 °C, a decline in red dye decontamination occurred when the heat treatment of boehmite was performed at longer times, >60 min. Though the powder calcined within 15 min indicated a removal efficiency ~97%, the adsorbents prepared in the longer soaking times were unable to effectively remove the blue dye. The plots imply that the calcination at 700 °C is proper to fabricate an adsorbent with the proper adsorptive performance in which soaking time should be considered at least 30 min.

2. Effect of Dye Solution pH on Removal Efficiency

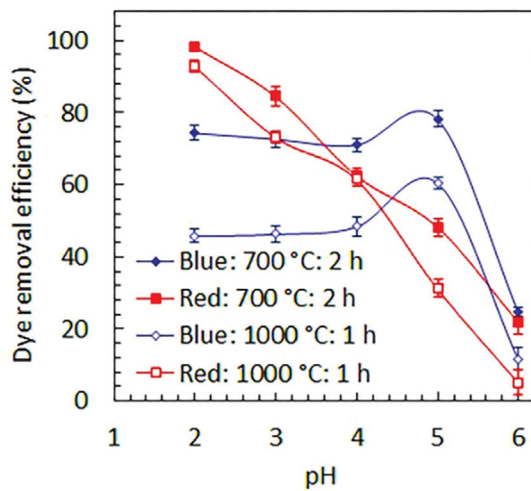The pH of wastewater is one of the most significant factors affect-

Fig. 3. Dye removal efficiency versus pH, calcination temperature: 700, and 1,000 °C, soaking time: 120 min, dye concentration: 200 mg L⁻¹, and adsorbent dosage: 0.50 g L⁻¹.

ing the dye removal efficiency through the change in the adsorbent surface charge. To analyze the influence of pH on dye adsorption, a detailed study was performed under different pH conducted from 2 to 6 as plotted in Fig. 3. In the acidic environment, the dye molecules have solvated as anions, which are the main predominating form. The anion adsorption from dye solution onto alumina particles is a pH dependent process due to affecting the adsorbent functional groups. Regardless of the calcination conditions, the pH should be adjusted at 5.0 to improve the electrostatic attraction between the positive surface of alumina particles and blue dye anions. The red dye removal efficiency also decreased in an abrupt manner from 98 to 22% due to change in pH in the range of 2-6 when the boehmite powder was calcined at 700 °C. The same trend in adsorption efficiency was observable for adsorbent produced at 1,000 °C.

3. Adsorption Isotherm

The equilibrium adsorption studies were conducted at 25 °C with different concentrations of dyes over the powder calcined in the proper condition, 700 °C within 30 min. As emphasized earlier, the increase in the calcination temperature significantly influenced the adsorption of dyes; as a result, the powder treated at 700 °C was used as a proper adsorbent in the equilibrium studies. Also, the pH of solutions contaminated by blue and red dyes was adjusted at 5.0, and 2.0, respectively, to maximize the adsorptive performance. As illustrated in Fig. 4, the adsorption performance improved with increase in the concentration, ensuring the saturation of active sites onto the alumina particles. Also, the maximal adsorption capacity indicates that the red dye is adequately adsorbed onto the alumina particles.

To address dye adsorption behavior over the alumina particles, different mathematical models were applied which are crucial to design the units for the removal of contaminants in practical conditions. A detailed insight about the adsorption process was obtained by applying three isotherms, Langmuir, Freundlich, and Temkin, which provided important information about the distribution of dye anions onto alumina-solution interface.
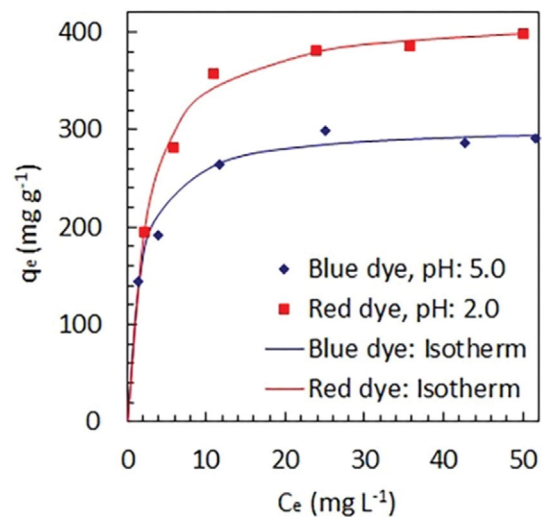
Fig. 4. Adsorption capacity versus blue, and red dye concentration, Langmuir isotherm for adsorbent produced by calcination at 700 °C within 30 min.

Langmuir: $\quad q_e = \dfrac{q_m K_L C_e}{1 + K_L C_e} \qquad$ or $\qquad \dfrac{C_e}{q_e} = \dfrac{1}{q_m K_L} + \dfrac{C_e}{q_m} \qquad$ (3)

Freundlich: $\quad q_e = K_F C_e^{1/n} \qquad$ or $\qquad \ln q_e = \ln K_F + \dfrac{1}{n} \ln C_e \qquad$ (4)

Temkin: $\quad q_e = \dfrac{R_g T}{b} \ln(A_T C_e) \quad$ or $\quad q_e = \dfrac{R_g T}{b} \ln A_T + \dfrac{R_g T}{b} \ln C_e \quad$ (5)

where C_e, and q_e denote the concentration and adsorption capacity in the equilibrium condition, respectively. q_m is the maximal adsorption capacity, and K_L is the Langmuir constant. K_F denotes the Freundlich constant, and $1/n$ is a power constant. A_B and b are Temkin isotherm, R_g is the universal gas constant, and T is absolute temperature. These models are the main isotherms which are frequently applied to obtain deep information about adsorbent ability. As seen in Table 2, the equilibrium data were better fitted by the Langmuir isotherm with higher coefficient of determination, R^2, as compared with those for Freundlich, and Temkin models,

Table 2. Parameters of isotherms for removal of blue, and red dyes at pH 5.0, and 2.0 over alumina powder calcined at 700 °C within 30 min

Isotherm	Parameter	Blue dye	Red dye
Langmuir	q_m (mg g⁻¹)	303	416.7
	K_L (L mg⁻¹)	0.60	0.42
	R^2	0.998	0.999
	R_L	0.02	0.03
Freundlich	n	5.00	4.52
	K_F	143.47	181.69
	R^2	0.910	0.882
Temkin	A_T (L mg⁻¹)	23.5	12.7
	b (J mol⁻¹)	57.2	38.3
	R^2	0.921	0.919

implying that monolayer adsorption occurred during the dye removal process. The prepared adsorbent exhibited an adsorption capacity of about 303, and 417 mg g^{-1} for the decontamination of solution polluted by blue, and red dyes, respectively, confirming that alumina powder produced from boehmite has the higher capacity to remove anionic dyes. The separation factor, R_L, was used to estimate the affinity between alumina powder and dyes in the monolayer adsorption, which can be predicted as:

$$R_L = \frac{1}{1+K_L C_0} \tag{6}$$

This factor represents the behavior of adsorption as irreversible if R_L is zero, favorable if $0<R_L<1$, linear if separation factor is equal to 1.0, and unfavorable when $R_L>1$. As reported in Table 2, R_L value for the removal of studied dyes is between zero and 1.0, which proves the favorable adsorption.

4. Industrial Wastewater Treatment

To study the practical application of produced alumina powder in the treatment of real systems, two industrial wastewaters contaminated by anionic blue and red dyes were collected from the recovery units of textile factories and were treated with fabricated adsorbent at the proper pHs, 5.0 and 2.0. The appropriate recovery could be achieved by using alumina powder as represented in Fig. 5 in which different dosages of absorbent were used to point out the effect of alumina powder on recovery of industrial wastewater. As shown, 45-50% of dyes was adsorbed by 1.7 g L^{-1} of adsorbent, which exhibits good performance in the recovery of real systems. With increment in the alumina dosage, the efficiency reached 90%. However, a little difference is observable in the performance of alumina powder, showing that the recovery of contaminated effluents could be carried out properly at the appropriate pHs.

5. Thermal Regeneration of Adsorbent

By taking account of secondary pollution due to deposition of spent adsorbent in the landfill, and cost of alumina, the regenera-

Table 3. Dye removal efficiency of thermally regenerated alumina powder for reusability evaluation in industrial wastewater treatment

Regeneration runs	Dye removal efficiency (%)	
	Blue	Red
Fresh	90.0±3.0	89.5±4.1
1	91.0±2.3	84.0±3.3
2	90.5±3.0	80.4±1.8
3	88.2±2.2	80.2±3.8
4	88.4±1.9	81.0±2.7
5	87.5±2.0	79.7±1.1
6	85.0±2.6	79.9±1.4
7	84.1±2.3	78.8±1.5
8	82.0±2.0	77.4±1.6
9	81.6±2.8	76.7±2.1
10	79.2±2.4	75.5±2.9

tion, and reusability are of great importance in the recovery of industrial wastewater. The absorption efficiency of alumina powder produced via the calcination at 700 °C towards the dye removal was evaluated up to ten regeneration cycles. To examine the reusability of adsorbent, the regenerated powder was mixed with industrial wastewater. Based on data reported in Table 3, the alumina powder could be easily regenerated by the thermal treatment at 500 °C.

A slight decline in the removal efficiency was found after each cycle, demonstrating an appropriate reusability. The alumina powder showed excellent performance after thermal regeneration in which the efficiency was still kept about 80-90% after five regeneration cycles, depending on dye chemical structure. Moreover, the adsorbent was not deteriorated after the wastewater treatment for multiple times. The major reason for the maintenance of adsorption yield is keeping the active sites in the thermal regeneration due to considerable difference between the fabrication and regeneration temperatures in which the structure remains intact approximately, demonstrating that alumina powder not only shows outstanding adsorption capacity, but also indicates the proper thermal stability.
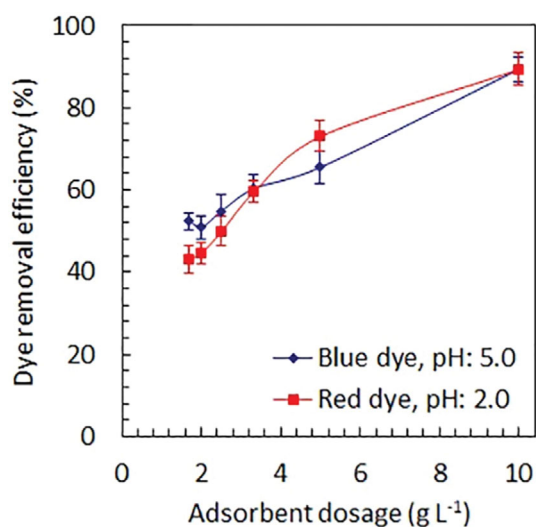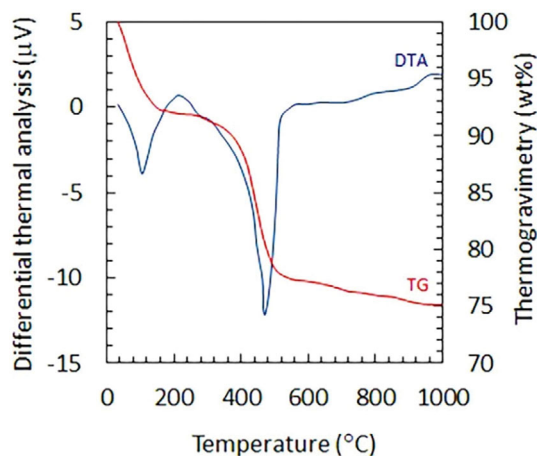

Fig. 5. Dye removal efficiency versus adsorbent dosage for recovery of industrial wastewater contaminated by blue, and red dyes, calcination temperature: 700 °C, soaking time: 30 min.

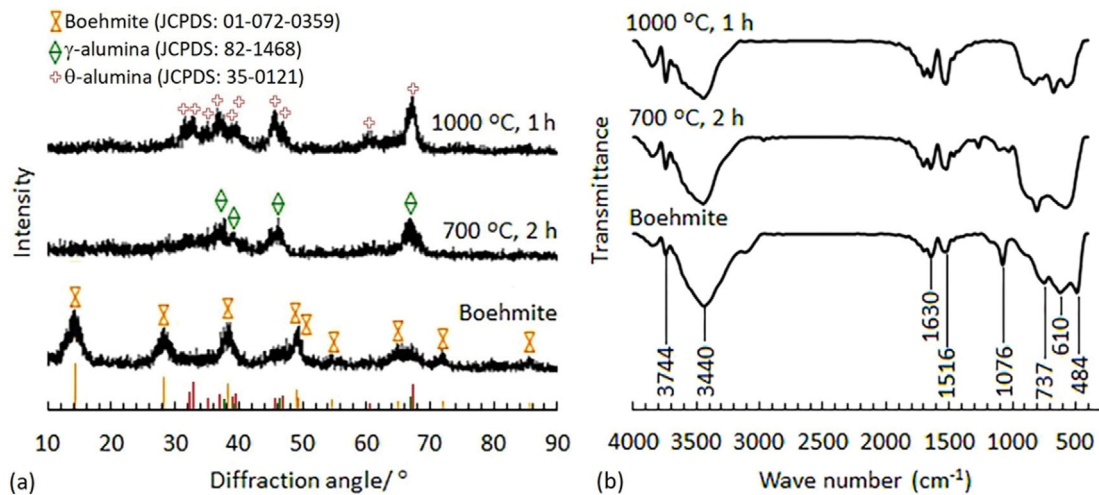Fig. 6. DTA-TG curves of used boehmite.

Fig. 7. Structural characteristics of boehmite and adsorbents, (a) XRD patterns, and (b) FTIR spectra.

6. Thermal Conversion of Boehmite

Fig. 6 indicates the DTA-TG curves of used boehmite for the production of adsorbents. Regarding the dehydration and dehydroxylation of boehmite, three stages were clearly identified. The first endothermic peak detected on the DTA curve corresponds to the dehydration of boehmite. The mass loss ~10% is observed in the temperature range of 30-150 °C, which is related to the evaporation of adsorbed water. In the temperature range of 300-560 °C, the second broad endothermic peak is assigned to dehydroxylation of boehmite. A mass loss about 14.8% was detected, which is close to the theoretical dehydroxylation of boehmite, 15%, leading to formation of γ-Al_2O_3. In the last stage, the mass of powder remains is unchanged up to 1,000 °C.

7. Crystalline and Chemical Structure of Adsorbents

The XRD pattern of boehmite and thermally treated powders is illustrated in Fig. 7(a). The refined crystalline phases are: boehmite for starting material, γ, and θ-Al_2O_3 for those treated at 700, and 1,000 °C, respectively. Boehmite diffractions were identified as broad peaks, indicating the formation of nano-crystallites. It is expected to find an evidence in the diffraction patterns of calcined powders. There is a change in the crystalline structure with an increase in the calcination temperature. The peaks at 45.5 and 67.1° are attributed to γ phase, while the diffractions at 32.8 and 67.4° are obviously related to θ phase. Although α-Al_2O_3 peaks were not detected, both patterns show appreciably wide peaks, which indicate poor crystalline structure. The crystallinity of γ and θ phases is lowest compared to the boehmite. Some reflections of γ-alumina are also observable in the pattern of powder calcined at 1,000 °C. This result is related to the structural transformation from cubic structure (γ-phase) to the monoclinic (θ-phase) structure. The crystalline nature of different phases is strongly dependent on the calcination condition. It is important to note that the DTA curve indicates no evidence for the transformation from γ into θ phase.

The FTIR spectra represented in Fig. 7(b) further demonstrate the structural change due to thermal treatment at 700, and 1,000 °C. The signals at 3,744 cm^{-1} are the characteristic absorption of Al-OH bond, and the broad vibration at 3,440 cm^{-1} is attributed to the absorption of hydroxyl group. The bending vibration at 1,630 cm^{-1} corresponds to O-H bond due to physically adsorbed water molecules. The weak signal at 1,516 cm^{-1} is ascribed to the vibration of carbonate group due to pollution of primary material. The peak at 1,076 cm^{-1} is ascribed to Al-O-H vibration in the AlO_4 group. The peaks in the wave number of 737, 610, and 484 cm^{-1} are related to the vibrations in AlO_6 group in boehmite. Although the mentioned signals in the spectra of calcined powders are similar to those observed in boehmite spectrum, the signal at 484 cm^{-1} was transformed to a broad band, indicating the formation of γ phase as illustrated by XRD patterns.

8. Microstructure of Adsorbents

The SEM images of adsorbents at 700, and 1,000 °C are represented in Fig. 8. A microscopic study revealed that the powder calcined at 700 °C mainly contains fine sized particles which were agglomerated, showing an irregular morphology, <10 µm (Fig. 8(a)). As expected, the form and size of agglomerates were preserved after heating at 1,000 °C, as represented in Fig. 8(b). The particles exhibit a similar microstructure with respect to the powder calcined at 700 °C with an evident intergrowth of boundaries due to strong calcination at the higher temperature.

Since the SEM micrographs are not sufficient to evaluate the adsorbent structure, FESEM tests were performed to deeply verify the crystalline transformation. In fact, high magnification image revealed the difference in the microstructure of thermally treated powders. The microstructure of alumina nanoparticles became clear, revealing the difference in the cleavages. The appropriate adsorption performance of powder prepared at 700 °C is related to the presence of spherical nanoclusters, <20 nm, as displayed in Fig. 8(c). The clusters represent the rough nature and sponge skeleton with an extended surface area, which allows better contact with the dye anions. The nanoclusters were fully transformed to semi-spherical particles with the size about 100 nm, Fig. 8(d), through thermal treatment at 1,000 °C. The intergrowth of spherical nanoparticles led to a sharp decline in the adsorption efficiency. The reduction in scavenging capacity is attributed to the weak interconnection with the surface of coarse particles.
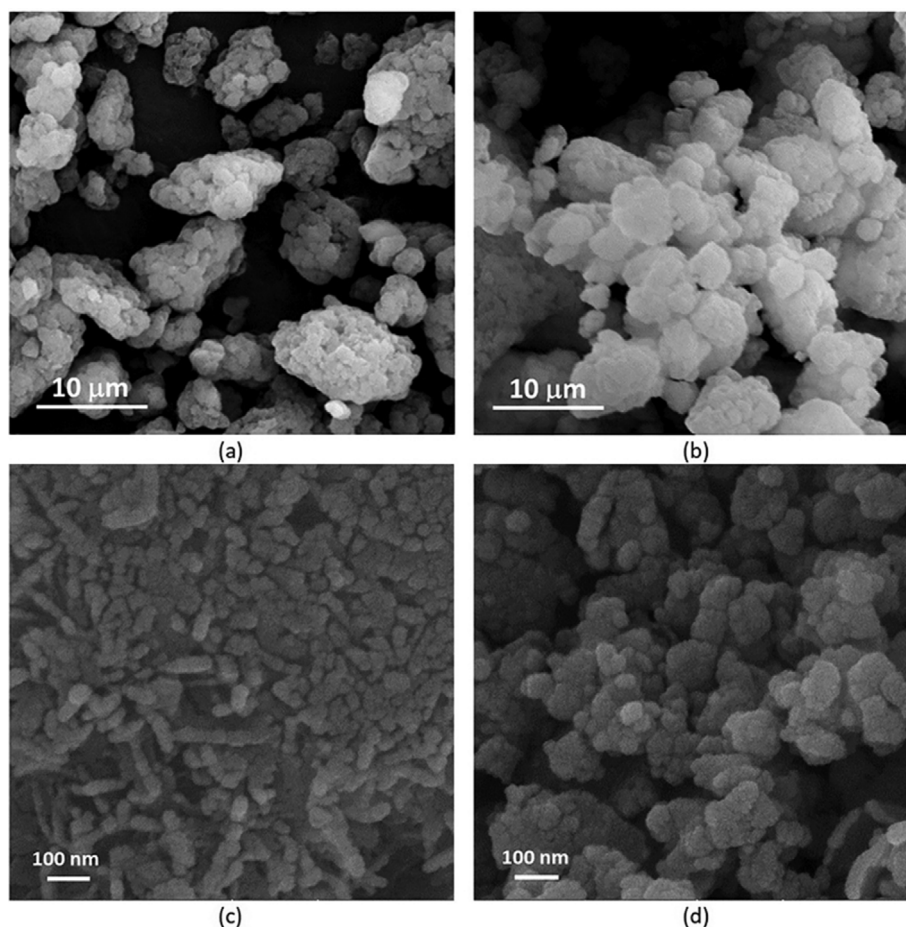
Fig. 8. Morphological features of adsorbents, SEM image of powders calcined at (a) 700 °C within 120 min, (b) 1,000 °C within 60 min, FESEM images of powders treated at (c) 700 °C within 120 min, and (d) 1,000 °C within 60 min.

9. Textural Characteristics of Adsorbents

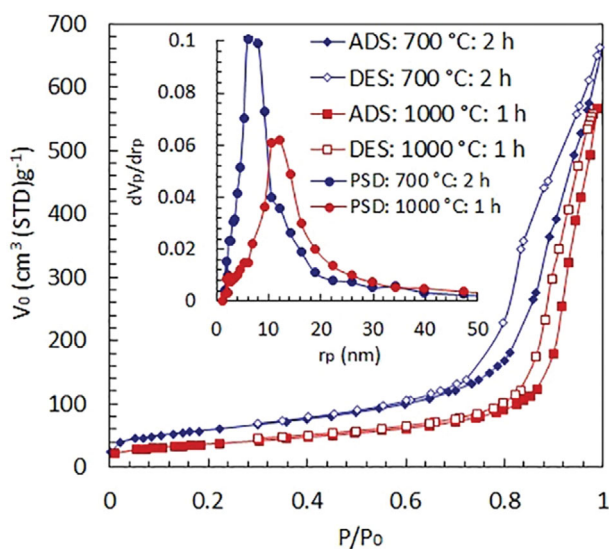The N$_2$ adsorption-desorption isotherms of powders prepared via calcination at 700 and 1,000 °C are displayed in Fig. 9. Although the plots are similar based on IUPAC nomenclature, the main difference is the nitrogen content adsorbed onto powders. Due to the sharp rise in the adsorption branches, which are barely noticeable at the higher relative pressures, close to 0.85, the isotherms are classified as type IV with hysteresis of H3, indicating a porous structure [30]. The type of isotherms and hysteresis loops remained unchanged with change in the calcination conditions. The powder calcined at 700 °C consists of micro and mesopores which were uniformly distributed in a narrow range, 2-20 nm, while the calcination at 1,000 °C led to a wide range distribution, 2-30 nm. The estimated pore sizes confirm the formation of mesoporous structure for both adsorbents. Additionally, the textural characteristics of alumina powders are reported in Table 4, indicating that the specific surface area and pore volume significantly declined after thermal treatment at 1,000 °C. On the other hand, the increase in the average mesopore diameter could be related to disappearance of micropores and association of mesopores. As is well known, a larger surface area supports the proper scavenging capacity.

The measured zeta potential of alumina powders is represented in Table 3 in which the adsorbents exhibit negative potential, meaning that the nanoparticles were charged negatively. The powder prepared at 700 °C represents a lower zeta potential than that pro-

Fig. 9. Nitrogen adsorption-desorption isotherms, and pore size distributions of alumina powders.

Table 4. Textural characteristics of powders calcined at different conditions

Temperature (°C)	Time (min)	Surface area ($m^2 \, g^{-1}$)	Pore volume ($cm^3 \, g^{-1}$)	Average pore size (nm)	Zeta potential (mV)
700	120	202.0	0.990	5.8	−1.6
1,000	60	126.0	0.880	12.0	−3.3

duced via the calcination at 1,000 °C, demonstrating that heat treatment at higher temperature increases the negative charge of nanoparticles, reducing the scavenging capacity.

10. Boehmite Conversion and Dye Adsorption Behavior

The change in adsorption properties with increase in calcination temperature is related to alteration in adsorbent structure. Based on DTA-TG curves, the dehydroxylation of used boehmite occurred at ~600 °C, confirming the transformation into γ-Al_2O_3 [31]. According to the XRD patterns, γ-Al_2O_3 is a unique phase formed with calcination up to 700 °C. The BET results indicate that the specific surface area of formed γ phase is about 202 $m^2 \, g^{-1}$, providing appropriate number of active sites. The adsorption of dyes onto γ-Al_2O_3 is an electrostatic phenomenon. Due to deprotonation of Al-OH bonds and formation of Al-O$^-$ groups, the surface of γ-

Al_2O_3 particles shows a negative charge at pH above 7.0, repelling the dye anions. When the pH of wastewater is lowered, the particle charge is changed due to protonation of Al-OH groups, leading to formation of Al-OH$_2^+$. On the other hand, the adsorption of dyes depends on the electrostatic attraction between Al-OH$_2^+$ species, and -NH, SO_3^{2-} groups in the chemical structure of anions as represented in Fig. 10. Not only is the number -NH bonds in the anions an effective factor in the adsorption of blue dye, but also the SO_3^{2-} groups play an essential role in the connection to Al-OH$_2^+$ species. Therefore, the red dye could be efficiently adsorbed because of containing more SO_3^{2-} groups compared to that for blue dye. Although the number of Al-OH$_2^+$ species increases with reduction in pH, a limited number of -NH, and SO_3^{2-} groups is available to connect Al-OH$_2^+$ species; consequently, the adsorption
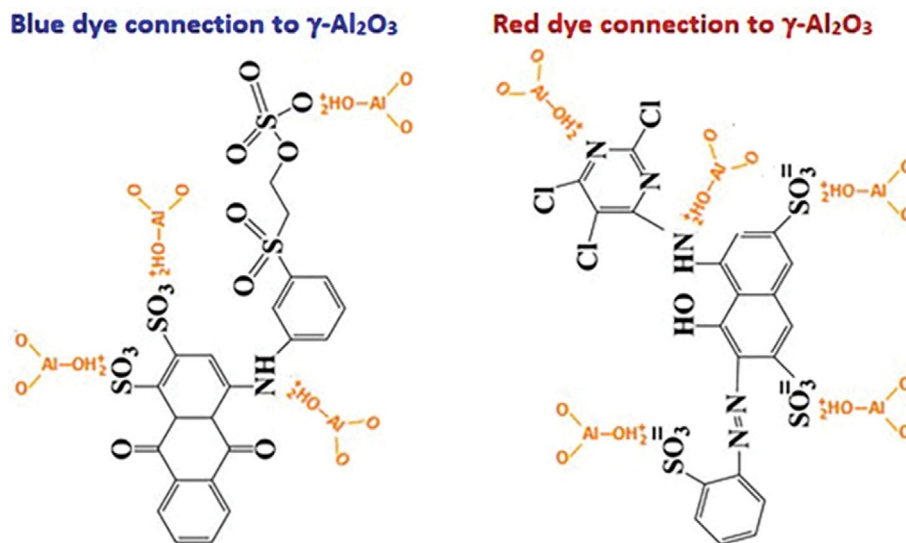
Fig. 10. Adsorption mechanism of blue and red dye onto γ-Al_2O_3 nanoparticles.

Table 5. Adsorption capacity of different adsorbents for removal of anionic dyes from wastewater

Dye	Adsorbent	Adsorption capacity ($mg \cdot g^{-1}$)	Reference
Reactive blue 2	Activated sludge	250.0	[34]
Reactive blue 19	Panus tigrinus biomass	13.7	[35]
Reactive blue 19	Modified silica gel	73.0	[36]
Reactive blue 4	Modified rice bran	185.2	[37]
Reactive blue 4	Phanerocheate chrysosporium fungus	211.6	[38]
Reactive blue 19	MgO	166.7	[39]
Reactive red 198	MgO	123.5	[39]
Reactive blue RS 150	MgO	1,000.0	[40]
Reactive blue RS 150	γ-Alumina	303.0	Present work
Reactive red RB 133	γ-Alumina	416.7	Present work

efficiency for blue dye remains constant in the pH range of 2-4. The ignition of dyes adsorbed onto alumina nanoparticles during the thermal regeneration process causes a local change in porous structure, vacancy distribution, and aggregation of nanoparticles, resulting in a decline in the number of active sites.

11. Future Research Perspectives and Cost Analysis

Different adsorbents were employed to remove anionic dyes from wastewater, as reported in Table 5. Although a variety of dyes were removed by adsorption, the proper capacity was reported for the nano-porous MgO produced based on template pathway and γ-Al$_2$O$_3$ fabricated in the present work. The preparation of γ-Al$_2$O$_3$ from boehmite led to achieving a reusable adsorbent with the higher adsorption capacity in the acidic condition. The results obtained in this study exhibit that the introduced method is desirable from an environmental point of view due to application in the corrosion condition. Moreover, the obtained alumina was thermally stable; consequently, it can be used for a longer time in wastewater treatment. The treatment of wastewater discharged from textile industries requires a multilateral consideration from shaping, calcination, and application in the fixed bed system in which mechanical strength and reliability are determinant factors. The adsorption system only can be coupled as supplemental process when dye concentration is lower than 20 mg L^{-1}, in the downstream of the treatment system to polish the discharged wastewater quality. The adsorption unit should be designed as a fixed bed system; however, due to the complexity, the forming of alumina adsorbent as rodlike shape was suggested in the previous work of authors [28]. Although the adsorption of anionic dyes onto the alumina powder was proved to be an effective way in wastewater treatment, the application of this process is still difficult, needing extended research to further prove the feasibility in the pilot scale from shaping point of view and adsorption in the dynamic condition. The direction of the current research is the initial cost analysis for recovery of an industrial wastewater with flow rate about 1.0 m^3 h^{-1}. These calculations were based on the proper content of adsorbent, 10 g L^{-1}, required to achieve the maximal efficiency, 90%. The boehmite powder was extracted from nepheline syenite ore in Iran, and the cost analysis was performed according to the starting material cost in 2022. Although the costs of shaping, calcination, and fixed bed construction should be considered, the main expense is related to the price of the starting material used for the fabrication of adsorbent. The treatment cost was estimated to be 2.2 US$ m^{-3} with 10 recycling runs.

CONCLUSIONS

The study dealt with a description of a pathway for the production of a thermally stable gamma alumina powder from boehmite for the decontamination of textile wastewater containing anionic dyes. The calcination of boehmite at 600-700 °C within 30 min can be considered as a safe procedure to achieve a reusable adsorbent for the decontamination of industrial textile wastewater without effectively losing adsorptive performance and creating secondary pollution. Note that the calcination of boehmite does not completely remove dyes. The significant performance was achieved with adjusting the pH of wastewater, depending on the chemical structure of the contaminant. The appropriate pH for the removal of blue and red dyes was found to be 5.0, and 2.0, respectively, in which the alumina structure remains unaffected at room temperature. The maximal adsorption capacities were determined as 303, and 416 mg g^{-1} for the remediation blue, and red dyes at the proper pHs, respectively. γ-Alumina with the proper mesopores, 6 nm, is a viable alternative for the removal of anionic dyes from wastewater because of chemical resistance, thermal stability, reusability, and simplicity of production.

REFERENCES

1. T. Xie, K. Chen, H. Xie, C. Miao, M. Yu, F. Li, Y. Chen, X. Yang, P. Li and Q. J. Niu, *Appl. Surf. Sci.*, **599**, 153914 (2022).
2. S. Zereshki, P. Daraei and A. Shokri, *J. Hazard. Mater.*, **356**, 1 (2018).
3. T. T. Lamminmäki, J. P. Kettle, P. J. T. Puukko and P. A. C. Gane, *Colloids Surf. A: Physicochem. Eng. Asp.*, **377**(1-3), 304 (2011).
4. F. Mcyotto, Q. Wei, D. K. Macharia, M. Huang, C. Shen and C. W. K. Chow, *Chem. Eng. J.*, **405**, 126674 (2021).
5. Y. Sun, D. Li, X. Lu, J. Sheng, X. Zheng and X. Xiao, *J. Environ. Manage.*, **299**, 113589 (2021).
6. M. Rezaei and Sh. Salem, *Int. J. Chem. Kinet.*, **48**(10), 573 (2016).
7. H. Jabkhiro, K. E. Hassani, M. Chems and A. Anouar, *Colloids Interface Sci. Commun.*, **45**, 100549 (2021).
8. W. Zhang, H. Li, X. Kan, L. Dong, H. Yan, Z. Jiang, H. Yang, A. Li and R. Cheng, *Bioresour. Technol.*, **117**, 40 (2012).
9. D. Sun, X. Zhang, Y. Wu and X. Liu, *J. Hazard. Mater.*, **181**(1-3), 335 (2010).
10. N. Atar, A. Olgun, S. Wang and S. Liu, *J. Chem. Eng. Data*, **56**(3), 508 (2011).
11. S. Şener, *Chem. Eng. J.*, **138**(1-3), 207 (2008).
12. E. Errais, J. Duplay, F. Darragi, I. M'Rabet, A. Aubert, F. Huber and G. Morvan, *Desalination*, **275**(1-3), 74 (2011).
13. E. Alver and A. U. Metin, *Chem. Eng. J.*, **200-202**, 59 (2012).
14. Y. An, H. Zheng, H. Zu, Y. Sun, Y. Wang, C. Zhao and W. Ding, *J. Hazard. Mater.*, **381**, 120971 (2020).
15. X. Zhang, Z. Li, S. Lin and P. Théato, *ACS Appl. Mater. Interfaces*, **12**(18), 21100 (2020).
16. Y. Li, F. Liu, H. Zhang, X. Li, X. Dong, G. Lu and C. Wang, *Mater. Lett.*, **238**, 183 (2019).
17. T. M. F. Marques, D. A. Sales, L. S. Silva, R. D. S. Bezerra, M. S. Silva, J. A. Osajima, O. P. Ferreira, A. Ghosh, E. C. S. Filho, B. C. Viana and J. M. E. Matos, *Appl. Surf. Sci.*, **512**, 145659 (2020).
18. P. Saharan, A. K. Sharma, V. Kumar and I. Kaushal, *Mater. Chem. Phys.*, **221**, 239 (2019).
19. X. Yu, C. Wei, L. Ke, Y. Hu, X. Xie and H. Wu, *J. Hazard. Mater.*, **180**(1-3), 499 (2010).
20. X. Y. Huang, X. Y. Mao, H. T. Bu, X. Y. Yu, G. B. Jiang and M. H. Zeng, *Carbohydr. Res.*, **346**(10), 1232 (2011).
21. W. Konicki, I. Pełech, E. Mijowska and I. Jasińska, *Chem. Eng. J.*, **210**, 87 (2012).
22. M. I. F. Macedo, C. A. Bertran and C. C. Osawa, *J. Mater. Sci.*, **42**, 2830 (2007).
23. V. V. Danilevich, O. V. Klimov, K. A. Nadeina, E. Y. Gerasimov, S. V. Cherepanova, Y. V. Vatutina and A. S. Noskov, *Superlattices Micro-*

struct., **120**, 148 (2018).

24. F. Karouia, M. Boualleg, M. Digne and P. Alphonse, *Adv. Powder Technol.*, **27**(4), 1814 (2016).

25. N. K. Renuka, A. V. Shijina and A. K. Praveen, *Mater. Lett.*, **82**, 42 (2012).

26. K. Nadafi, M. Vosoughi, A. Asadi, M. O. Borna and M. Shirmardi, *J. Water Chem. Technol.*, **36**(3), 125 (2014).

27. S. Banerjee, S. Dubey, R. K. Gautam, M. C. Chattopadhyaya and Y. C. Sharma, *Arab. J. Chem.*, **12**(8), 5339 (2019).

28. A. H. Razm, A. Salem and Sh. Salem, *J. Hazard. Mater.*, **429**, 128259 (2022).

29. M. Malakootian, H. Jafari Mansoorian, A. R. Hosseini and N. Khanjani, *Process. Saf. Environ.*, **96**, 125 (2015).

30. M. Thommes, K. Kaneko, A. V. Neimark, J. P. Olivier, F. Rodriguez-Reinoso, J. Rouquerol and K. S. W. Sing, *Pure Appl. Chem.*, **87**(9-10), 1051 (2015).

31. X. Zhang, P. L. Huestis, C. I. Pearce, J. Z. Hu, K. Page, L. M. Anovitz, A. B. Aleksandrov, M. P. Prange, S. Kerisit, M. E. Bowden, W. Cui, Z. Wang, N. R. Jaegers, T. R. Graham, M. Dembowski, H.-W. Wang, J. Liu, A. T. N'Diaye, M. Bleuel, D. F. R. Mildner, T. M. Orlando, G. A. Kimmel, J. A. La Verne, S. B. Clark and K. M. Rosso, *ACS Appl. Nano Mater.*, **1**, 7115 (2018).

32. H. V. Gog, *Appl. Surf. Sci.*, **541**, 148501 (2021).

33. S. Ali, Y. Abbas, Z. Zuhra and I. S. Butler, *Nanoscale Adv.*, **1**, 213 (2019).

34. Z. Aksu, *Biochem. Eng. J.*, **7**, 79 (2001).

35. M. M. Mustafa, P. Jamal, M. Alkhatib, S. S. Mahmod, D. N. Jimat and N. N. Ilyas, *Electron. J. Biotechn.*, **26**, 7 (2017).

36. A. Banaei, S. Samadi, S. Karimi, H. Vojoudi, E. Pourbasheer and A. Badiei, *Powder Technol.*, **319**, 60 (2017).

37. G. B. Hong and Y. K. Wang, *Appl. Surf. Sci.*, **423**, 800 (2017).

38. G. Bayramoglu, G. Celik and M. Y. Arica, *J. Hazard. Mater.*, **137**, 1689 (2006).

39. G. Moussavi and M. Mahmoudi, *J. Hazard. Mater.*, **168**, 806 (2009).

40. S. Pourrahim, A. Salem, Sh. Salem and R. Tavangar, *Environ. Pollut.*, **256**, 113454 (2020).